Journal of Thermal Analysis and Calorimetry, Vol. 92 (2008) 1, 109–114

CRYSTAL STRUCTURE AND THERMOANALYTICAL STUDY OF A MANGANESE(II) COMPLEX WITH 1-ALLYLIMIDAZOLE

S. De Angelis Curtis[1], *Krystyna Kurdziel*[2], *S. Materazzi*[1] *and S. Vecchio*[3*]

[1]Department of Chemistry, University of Rome 'La Sapienza', P.le A. Moro 5, 00185 Rome, Italy
[2]Institute of Chemistry, Świętokrzyska Academy, Checinska 5, 25-020 Kielce, Poland
[3]Department of Chemical Engineering (I.C.M.A.), University of Rome 'La Sapienza, Via del Castro Laurenziano 7, 00161 Rome, Italy

The crystal structure of a manganese(II) 1-allylimidazole complex ($[Mn(1\text{-}AIm)_3(NO_3)_2]$, where 1-Aim=1-allylimidazole), was characterized by X-ray diffraction (XRD) using SHELX-97. The thermal behaviour of the complex was investigated by thermogravimetry (TG) coupled with an FTIR unit. The complex showed a multi-step decomposition related to the release of the ligand molecules, followed by oxidation. The final residue at 1073 K was found to be manganese(II) oxide. Evolved gas analysis allowed to prove the oxidative decomposition pattern of the examined complex, initially proposed by the percentage mass loss data. Finally, a kinetic analysis of the oxidative decomposition steps was made using the Kissinger equation, while the complex nature of the decomposition kinetics was revealed by the isoconversional Ozawa–Flynn–Wall method.

Keywords: *coordination compound, coupled TG-FTIR, crystal structure, decomposition kinetics, DSC, EGA, imidazole derivatives, TG, XRD*

Introduction

Imidazole and its derivatives are among the most important classes of molecules for their applications in biology (e.g., biocatalysis) and industry (e.g., as effective corrosion inhibitors or hidden curing agents for epoxy resins [1]). Therefore, coordination compounds of imidazole derivatives with transition metal ions, whose structures are characterized by single crystal X-ray technique [2], are suitable to study different aspects of biological molecules and industrial application. Recently, spectral and magnetic behaviour as well crystal structure and thermal decomposition of Mn(II) complexes were investigated using several techniques in conjunction with thermal analysis techniques [3, 4], while thermal analysis only was used to study the thermal decomposition of diguanide complexes [5] and inclusion compounds of microporous manganese formate [6]. Mn(II) complexes with imidazole derivatives were synthesized by several authors focusing their attention mainly on the structural properties [7–10]. Recently, thermal behaviour of imidazole derivatives complexes with divalent transition metal ions was also investigated by different authors [11–13]. However, recently our research group has been involved in the kinetic study of the decomposition of some imidazole derivatives complexes that undergo multi-step processes when they are submitted to a programmed rising temperature heating [14–16] under a controlled air atmosphere. As a continuation of this research the crystal structure and the thermal behaviour of a Mn(II) complex with 1-allylimidazole is described in this work by using different techniques: X-ray diffraction (XRD) spectroscopy, thermogravimetry (TG) and first-order thermogravimetry (DTG) and TG unit coupled with FTIR spectroscopy by means of a heated transfer line in a proper temperature range up to 450 K (TG-FTIR). A possible degradation pathway is proposed for all the degradation steps according to the mass losses recorded by the TG unit, and a substantial confirmation is obtained with the TG-FTIR evolved gas analysis.

Experimental

Materials

The 1-allylimidazole, propan-2-ol, trimethyl *ortho*-formate and $Mn(NO_3)_2{\cdot}H_2O$ were purchased from Aldrich Chemical Co. and were used without further purification, while the solvents used were RPE grade.

The complex studied was obtained from the same mixture of solvent. 25 cm^3 of the solution containing 0.2230 g $Mn(NO_3)_2{\cdot}H_2O$ was gradually added with constant stirring to a 25 cm^3 solution of 1-allylimidazole (4 mmol). The solution was left to stand at room temperature for a few days and the resulting crystals were filtered and washed with cold diethyl ether. The colourless crystals produced were suitable for X-ray

* Author for correspondence: stefano.vecchio@uniroma1.it

1388–6150/$20.00
© 2008 Akadémiai Kiadó, Budapest
Akadémiai Kiadó, Budapest, Hungary
Springer, Dordrecht, The Netherlands

diffraction study. Elemental analysis data of the complex considered in this study were summarized as follows: C 43.2% (43.0), H 4.6% (4.8), N 22.3% (22.3). As a result of the excellent agreement between experimental and calculated data (in brackets) a general formula $[Mn(1\text{-}Aim)_3(NO_3)_2]$ can be hypothesized.

Instrumental methods

Elemental analysis was performed by a VarioEl III CHN Analyzer; X-ray measurements were performed on a Kuma KM4CCD diffractometer; the structures were solved by direct methods using the SHELX-97 [17] and refined by full-matrix least-squares methods using the SHELXL-97 [18] programme.

The TG curves were recorded using a Perkin-Elmer TGA7 equipment in the temperature range between 20 and 800°C, the atmosphere was pure nitrogen or air under a flow rate of 100 mL min^{-1}; TG experiments were carried out using 7–8 mg of sample at several heating rates between 2.5 and 20 K min^{-1} for the kinetic study, while the thermal behaviour was investigated using TG data at 10 K min^{-1} because of its best resolution. IR spectra of the gases evolved during the experiments were recorded since the TG apparatus was coupled with a Perkin-Elmer FTIR spectrometer, model 1760X. The TGA7 was linked to the heated gas cell of the FTIR instrument by means of a heated transfer line, the temperatures of the cell and of the transfer line being independently selected.

Kinetic method of calculation

The methods proposed in this study are based on the assumption that kinetic parameters do not depend on the selected heating rate. The basic kinetic equation is

$$d\alpha/dt = k(T)f(\alpha) \quad (1)$$

where t is the time, α is the fraction decomposed defined as $\alpha=(w_i-w_T)/(w_i-w_f)$, $f(\alpha)$ is the model function, which assumes different mathematical forms depending on the reaction mechanism [19] and $k(T)$ is the specific rate constant, whose temperature dependence is commonly described by the Arrhenius equation:

$$k(T) = A\exp(-E/RT) \quad (2)$$

where E is the activation energy, A is the pre-exponential factor, R the gas constant and T the absolute temperature. Moreover, taking into account that under non-isothermal condition the heating rate $\beta=dT/dt$, $d\alpha/dt=d\alpha/(dT/\beta)$, combining Eqs (1)–(2), gives:

$$d\alpha/dT = (A/\beta)\exp(-E/RT)\cdot f(\alpha) \quad (3)$$

However, due to the complexity of the kinetic description concerning the solid state decomposition processes it is usually assumed that the activation energy is not a constant value but depends on α [20, 21]. Therefore, in order to establish if such dependence exists or not, the kinetic procedure adopted in this work was firstly based on two multi-heating rates methods. Both approaches determine the activation energy using thermal analysis data carried out at different fixed heating rates without choosing a priori a defined model function. In particular, the first kinetic method used was Kissinger method [22] that uses the following equation:

$$\ln(\beta/T_m^2) = \ln[(AR)/E] + (-E/R)(1/T_m) \quad (4)$$

where T_m is the DSC peak temperature at a given heating rate β. From the slope of Eq. (4) a single activation energy value for each step of mass loss is given. In order to test the dependence of activation energy on the fraction decomposed α the isoconversional method of Ozawa–Flynn–Wall (OFW) [23, 24] was also considered. This method is based on the integral form of Eq. (1) according to the following isoconversional equations

$$\ln(\beta)_\alpha = \ln[(A_\alpha R)/E_\alpha] - \lg(\alpha) - 5.3305 - 1.052(E_\alpha/R)(1/T_\alpha) \quad (5)$$

Once the Doyle's approximation [25]: $\ln p(x) \approx -5.3305 - 1.052x$, where $x=E_\alpha/(RT_\alpha)$ and $20 \le x \le 60$) is verified to be valid over the entire range of α, then at any selected value of α, from the slope of the related regression straight line derived by the $\ln(\beta)_\alpha$ *vs*. $1/T_\alpha$ plot, the corresponding E_α value is derived as a function of α.

Results and discussion

Crystal structure analysis

Details of the crystal data and refinement for the manganese(II) complex investigated are collected in Table 1. The neutral complex $[Mn(1\text{-}Aim)_3(NO_3)_2]$ is made up of three molecules of 1-allylimidazole and two nitrate groups placed in the coordination sphere of the central ion. The labelling of the atoms and the structure of the complex is shown in Fig. 1. The azole ligands are connected with the central ion through the endocyclic nitrogen atoms of the 1,3-diazole ring. Selected bond distances and angles are given in Table 2. The manganese-nitrogen bond lengths are: Mn–N(1) 2.197(3) Å, Mn–N(3) 2.229(5) Å. They are slightly longer than the corresponding bonds in the analogous cobalt(II) complex, (2.098(2), 2.196(3) Å), and the nickel(II) one, (2.052(2) Å) [26]. The nitrate groups in the present complex are chelating bi-dentate ligands. The manganese-oxygen bond lengths are 2.326(3) and 2.347(2) Å. The difference in the

Table 1 Crystal data and structure refinement for complex $[Mn(1\text{-}AIm)_3(NO_3)_2]$

	$[Mn(1\text{-}AIm)_3(NO_3)_2]$
Empirical formula	$C_{18}H_{24}MnN_8O_6$
Molecular mass	503.39
Temperature/K	100(1)
Radiation	Mo Kα (λ= 0.71073 Å)
Crystal system	Monoclinic
Space group	C2/c
a/Å	19.176(4)
b/Å	12.434(3)
c/Å	10.562(2)
β/°	113.82(3)
V/Å^3	2303.9(8)
Z	4
μ/mm^{-1}	0.624
2θ range/°	3.65–26.00
Data [I>2σ (I)]/parameters	1916/183
Reflections collected	6996
Independent reflections	2247, [R(int)=0.0359]
Final *R*1, *wR*2 [I>2σ (I)]	0.0569, 0.1443
Largest differential peak and hole *e*/Å^{-3}	0.940 and –0.472

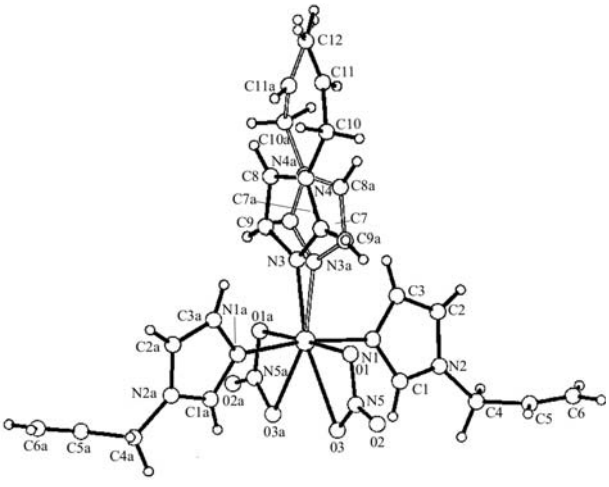

Fig. 1 The structure and numbering scheme for manganese(II) complex, $[Mn(1\text{-}AIm)_3(NO_3)_2]$

lengths of these bonds is not more than 0.02 Å, so they are then symmetric bonds. The opposite situation occurs in the analogous cobalt(II) and nickel(II) complexes with 1-allylimidazole. Asymmetry in the metal-oxygen bond lengths is observed in these compounds, i.e. the asymmetry of these bonds is 0.41 Å in the cobalt(II) complex $[CoL_3(NO_3)_2]$, and

Table 2 Selected bond lengths (Å) and angles (°) for complex $[Mn(1\text{-}AIm)_3(NO_3)_2]$

Bond lengths/Å			Bond angles/°
Mn–N(1)	2.197(3)	N(1)–Mn–N(1a)	172.6(1)
Mn–N(3)	2.229(5)	N(1)–Mn–N(3a)	94.5(6)
Mn–O(1)	2.326(3)	N(1)–Mn–N(3)	92.9(6)
Mn–O(3)	2.347(2)	N(1)–Mn–O(1)	92.7(1)
O(1)–N(5)	1.266(4)	N(1)–Mn–O(1a)	88.1(1)
O(2)–N(5)	1.228(4)	N(3)–Mn–O(1)	90.2(2)
O(3)–N(5)	1.259(4)	N(3)–Mn–O(1a)	78.3(2)
		O(1)–Mn–O(1a)	168.5(2)
		N(1)–Mn–O(3)	87.3(1)
		N(1a)–Mn–O(3)	87.1(1)
		N(3a)–Mn–O(3)	133.1(2)
		N(3)–Mn–O(3)	145.0(2)
		O(1)–Mn–O(3)	54.9(1)
		O(1a)–Mn–O(3)	136.6(1)
		N(1)–Mn–O(3a)	87.1(1)
		O(3)–Mn–O(3a)	81.8(1)

0.44 Å in the nickel(II) one [26]. The difference in the length of metal-oxygen bonds of the nitrate group (Ni-O(1); 2.093(2), Co-O(1); 2.196(3), Mn-O(1); 2.3263(3) Å) is related to the different angles of the N(5)–O(1)–metal bonds, i.e. the angles are 105.4(2), 99.8(2), 94.4(2) for the complexes of nickel(II), cobalt(II) and manganese(II), respectively. The agreement of the increase in the asymmetry of the metal-oxygen bonds, (Mn(II)<Co(II)<Ni(II)), is observed in the present complexes when the radius of the central metal ion becomes shorter [27, 28]. The angles of the oxygen-manganese-oxygen bond are 54.9(1)° in each group. As a result of the contribution of the oxygen atoms O(1) and O(3) of the nitrate group in the bond with the central ion, the angle O(3)–N(5)–O(1) (from the trigonal value) is reduced to 117.0(3)°. The successive angles of oxygen-nitrogen-oxygen bonds in the nitrate groups (O(1)-N(5)–O(2) 121.5(4)° and O(2)-N(5)-O(3)) are 121.5(4)°. One of the three molecules of 1-allylimidazole present in the complex is placed at the double axis of the complex, with half-occupancy (the occupancy factor *G*=0.5). The immediate environment of the central manganese ion in the present complex is made up of three nitrogen atoms of heterocyclic rings and four oxygen atoms of nitrate groups – the seven-coordination complex (MnN_3O_4). In this complex, there are namely two nitrogen atoms, N(1) and N(1a) and two oxygen atoms O(1) and O(1a) as occupying corners of the square plane. The remaining two oxygen atoms O(3) and O(3a) occupy one of the axial sites of this coordination polyhedron, whereas the other one is occupied by the nitrogen atom N(3).

The angle between the plane of the molecule of 1-allylimidazole N(3), N(4), C(7), C(8), C(9) and the plane determined by the atoms labelled N(1), N(2), C(1), C(2), C(3) is 89.7(2)°, and the plane of the nitrate group (O(1), O(2), O(3), N(5)) is 16.0(5)°.

Thermal, evolved gas and kinetic analyses

Figure 2 shows the TG/DTG curves of the complex studied in air flow, where three steps of mass loss are observed. The temperature ranges and the percentages of mass loss determined by the TG curves are given in Table 3. The first step, which begins at about 120°C, is ascribed to the loss of both the nitrate groups similarly to what it has been previously described for other 1-allylimidazole complexes of divalent metal ions [29] having nitrate groups inside or outside the coordination sphere of the central atom. The second noticeable step of mass loss, which occurs between 200 and 250°C, is clearly attributable to the loss of the three ligand molecules, followed by the third final step of mass loss due to oxidation to give the manganese(II) oxide, as confirmed by the X-ray diffraction spectra (not shown) carried out on a sample treated at 1000°C. The percentage of mass loss data found by TG experiments were compared in Table 3 with those calculated taking into account the above-mentioned mechanisms proposed. The excellent agreement obtained confirms the reliability of the suggested thermal decomposition pathway.

The TG-FTIR evolved gas analysis allows to confirm the proposed decomposition mechanism. From the stacked plot, there is a clear evidence of the

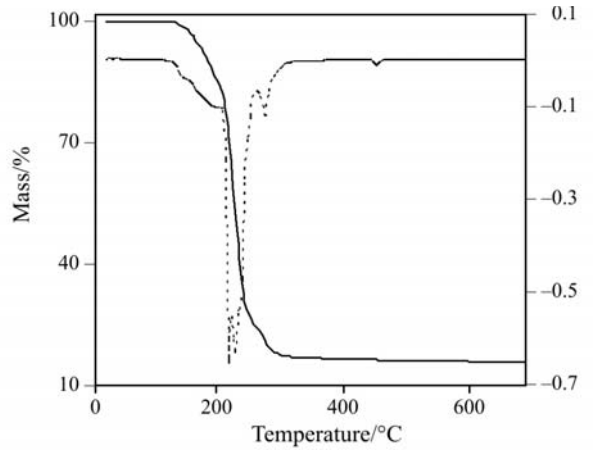

Fig. 2 TG (—) and DTG (---) curves of $[Mn(1\text{-}AIm)_3(NO_3)_2]$ complex. Heating rate: 10°C min^{-1}; air flow at 100 mL min^{-1} rate

Table 3 Results of the TG measurements carried out under an air flowing atmosphere (100 mL min^{-1}) at 10°C min^{-1}

Step	ΔT/°C	Mass loss/%	
		Calc.	Found
I	118–202	16.3	16.7
II	202–252	56.9	56.9
III	252–600	10.1	10.1

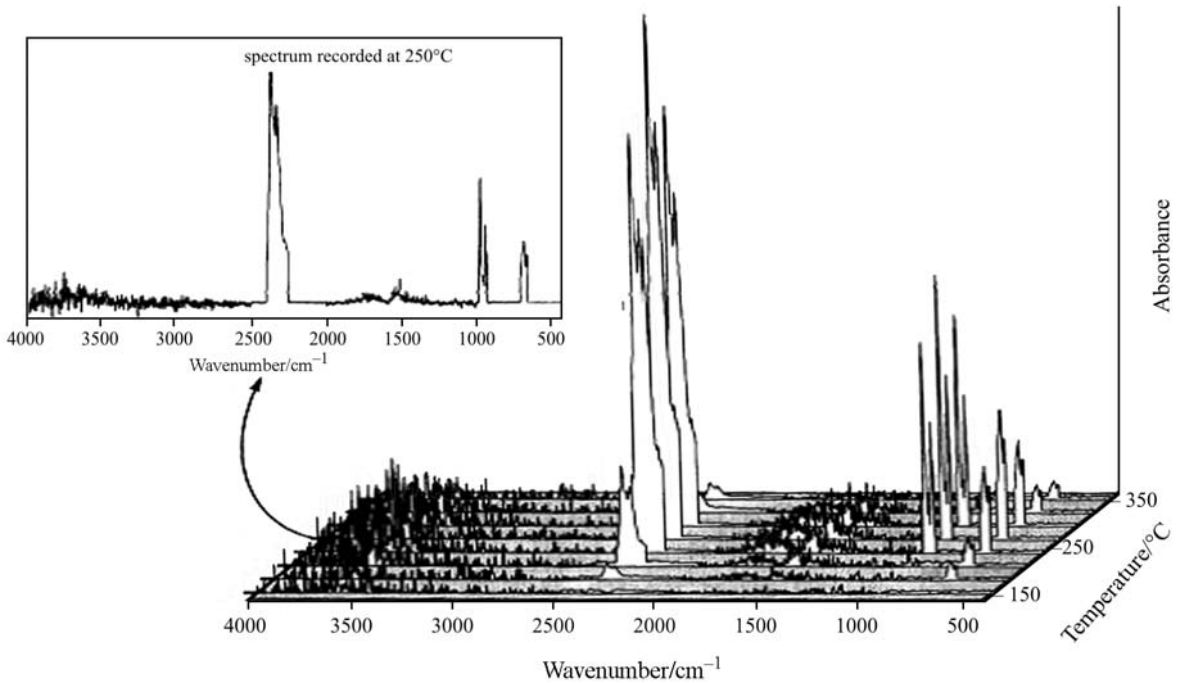

Fig. 3 Infrared spectra of the evolved gases for the thermal decomposition of the $[Mn(1\text{-}AIm)_3(NO_3)_2]$ complex in the temperature range 150–350°C. Resolution: 8 cm^{-1} –10 scans per spectrum

complete decomposition of the ligand molecules because of the absence of IR bands due to the loss of alkyl side-chains (Fig. 3).

The kinetic parameters associated to each decomposition step obtained from the slopes and intercepts of a regression line applied to Eq. (4) are listed in Table 4 along with the regression coefficients and the R^2 values. The activation energy values calculated using the Kissinger method largely differ from one step to another, thus revealing the complex nature of the decomposition processes examined. Its dependence on the fraction decomposed α, as determined using Eq. (5) (OFW method), is shown in Fig. 4. Compared with the associated errors a rather small decrease of E values (from 109 to 75 kJ mol^{-1}) is found in the first decomposition step, followed by an increase of the same extent (from 72 to 111 kJ mol^{-1}) at the beginning of the second decomposition step ($0.2<\alpha<0.4$), while practical constant E values (around 110 kJ mol^{-1}) are observed up to $\alpha<0.8$. The third decomposition step is characterized by a very large increase of activation energy up to about 300 kJ mol^{-1} accompanied by large errors (about ±60 kJ mol^{-1}).

On the other hand, both the E and ln$A$ values determined by the Kissinger method (Table 4) increase from the first to the third decomposition step. Taking into account the Arrhenius equation, these trends of E values should suggest a decreasing trend of the corresponding rate constants, while for that of ln$A$ an increasing trend of the rate constants should be hypothesized. Therefore, in order to establish which the rate determining decomposition step is, the rate constants ($k<T>$) for all decomposition steps were

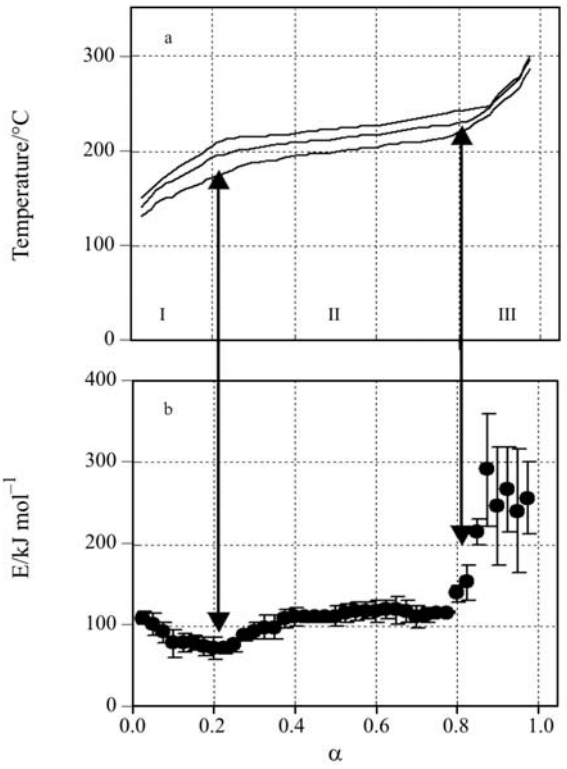

Fig. 4 TG curves of $[Mn(1\text{-}AIm)_3(NO_3)_2]$ at 2.5, 5 and 10 K min^{-1} (a – curves from down to up, respectively) compared with b – the α-dependence of activation energy

Table 5 Comparison of kinetic rate constant values for the thermal decomposition processes of some 1-allylimidazole complexes

Complexes (Lit.)	step	$k<T>$/min^{-1}[a,b,c]
$[Mn(1\text{-}AIm)_3(NO_3)_2]$ (This study)	I	$2.33\cdot10^{-1}$
	II	$6.58\cdot10^{-1}$
	III	$1.03\cdot10^{-1}$
$CoL_4(NO_3)_2$[d] (9)	I	$3.43\cdot10^{-4}$
	II	$4.03\cdot10^{-3}$
	III	$3.69\cdot10^{-1}$
$NiL_4(NO_3)_2$[d] (9)	I	$5.78\cdot10^{-1}$
	II	$2.38\cdot10^{-1}$
	III	$4.36\cdot10^{-1}$
$CuL_4(NO_3)_2$[d] (9)	I	$2.12\cdot10^{-4}$
	II	$1.98\cdot10^{-3}$
	III	$1.32\cdot10^{0}$
$[PdL_4]Cl_2\cdot3H_2O$[e,f] (10)	I	$4.22\cdot10^{-6}$
	II	$8.73\cdot10^{-3}$
	III	$7.63\cdot10^{-2}$
$[PdL_4]Cl_2\cdot3H_2O$[e,g] (10)	I	$1.87\cdot10^{-6}$
	II	$6.25\cdot10^{-11}$
	III	$8.10\cdot10^{-2}$

[a]The associated uncertainty (standard deviations) are always lower than 10%; [b]$<T>$=average of the experimental temperature range considered; [c]Calculated using the Arrhenius parameters taken from the paper cited in parentheses; [d]L=4(5)-hydroxymethyl-5(4)-methylimidazole; [e]L=1-allylimidazole; [f]complex 2a; [g]complex 2b

Table 4 Regression and Arrhenius parameters for the decomposition processes by the Kissinger method

Step	$\ln(\beta/T_m^2)=a+b\cdot10^3\cdot T_m^{-1}$		R^2	E/kJ mol^{-1}[a]	ln(A/min^{-1})[a]
	A[a]	B/K[a]			
I	13.5±1.8	–10.5±0.8	0.9947	87±6	22.7±1.7
II	19.8±1.6	–15.0±0.8	0.9977	124±4	29.4±0.8
III	22.7±1.1	–17.4±0.6	0.9988	144±3	32.5±1.1

[a]The associated uncertainty are standard deviations

calculated at the average of the experimental temperature range investigated using the Arrhenius equation. The derived $k<T>$ values were compared in Table 5 with those associated to decomposition steps of selected imidazole derivative complexes of divalent metal ions, whose Arrhenius parameters were taken from literature [14, 15]. The rate determining step seems to be the first one, while the third one show the higher $k<T>$ value (also when compared with those of the other complexes). The increasing trend of $k<T>$ values observed in the complexes considered (with the exception of both $NiL_4(NO_3)_2$ and $[PdL_4]Cl_2{\cdot}3H_2O$, complex 2b) may be largely attributed to the increasing trend of the $<T>$ values from the first to the third step.

Conclusions

The present study confirmed that the coupling of TG and DTG with supplementary techniques, such as XRD and FTIR enable the crystal structure and the thermal behaviour of complexes to be investigated as well as the decomposition pathways and their kinetic characteristics to be completely defined.

Supplementary data

Detailed crystal data and structure refinement for complex $[Mn(1\text{-}Aim)_3(NO_3)_2]$ have been deposited with the Cambridge Crystallographic Data Centre under No. CCDC663976. Copies of this information may be obtained free of charge from The Director, CCDC, 12 Union Road, Cambridge, CB2 IEZ, UK (fax:+44 1223 336033; e-mail: deposit@ccdc.cam.ac.uk or http://www.ccdc.cam.ac.uk).

References

1 V. I. Kalmykov and V. A. Ivanov, Zh. Prikl. Khim., 52 (1979) 889
2 K. Kurdziel and T. J. Glowiak, Coord. Chem., 55 (2002) 327.
3 W. Ferenc, B. Bocian and J. Sarzynski, J. Therm. Anal. Cal., 84 (2006) 377.
4 Q. Yang, S. Chen and S. Gao, J. Therm. Anal. Cal., 89 (2007) 567.
5 R. Olar, M. Badea, E. Cristurean, C. Parnau and D. Marinescu, J. Therm. Anal. Cal., 84 (2006) 53.
6 V. Logvinenko, D. Dybtsev, V. Fedin, V. Drebushchak and M. Yutkin, J. Therm. Anal. Cal., 90 (2007) 463.
7 D. Das, B. G. Chand, J. S. Wu, T. –H. Lu and C. Sinha, J. Mol. Struct., 842 (2007) 17.
8 G. Mago, M. Hinago, H. Miyasaka, N. Matsumoto and H. Okawa, Inorg. Chim. Acta, 254 (1997) 145.
9 O. Z.Yesilel, H. Olmez and H. Icbudak, J. Therm. Anal. Cal., 89 (2007) 555.
10 P. Naumov, G. Jovanovski and A. Todorovska, J. Mol. Struct., 563–564 (2001) 341.
11 K. Kurdziel, T. Glowiak, S. Materazzi and J. Jezierska, Polyhedron, 22 (2003) 3123.
12 M. Olczak-Kobza, R. Czylkowski and J. Karolak-Wojciechowska, J. Therm. Anal. Cal., 74 (2003) 895.
13 W. Wolodkiewicz, J. Therm. Anal. Cal., 68 (2002) 141.
14 S. Materazzi, S. Aquili, S. De Angelis Curtis, S. Vecchio, K. Kurdziel and F. Sagone, Thermochim. Acta, 421 (2004) 19.
15 S. Vecchio, S. Materazzi and K. Kurdziel, Int. J. Chem. Kin., 37 (2005) 667.
16 S. Materazzi,, S. Aquili, S. Vecchio and K. Kurdziel, Thermochim. Acta, 457 (2007) 7.
17 G. M. Sheldrick, SHELXS 97, Program for Solution of Crystal Structure, University of Göttingen, Germany, 1997.
18 G. M. Sheldrick, SHELXL 97, Program for Refinement of Crystal Structure, University of Göttingen, Germany, 1997.
19 X. Gao, D. Chen and D. Dollimore, Thermochim. Acta, 223 (1993) 75.
20 S. Vyazovkin and C. A. Wight, Ann. Rev. Phys. Chem., 48 (1997) 119.
21 A. K. Galwey and M. E. Brown, Thermal Decomposition of Ionic Solids, Elsevier, Amsterdam, 1999.
22 H. E. Kissinger, Anal. Chem., 29 (1957) 1702.
23 J. H. Flynn and L. A. Wall, J. Polym. Sci. B: Polym. Lett., 4 (1966) 323.
24 T. Ozawa, Bull. Chem. Soc. Jpn., 38 (1965) 1881.
25 C. D. Doyle, J. Appl. Polym. Sci., 6 (1962) 639.
26 K. Kurdziel and T. Głowiak, J. Mol. Struct., 516 (2000) 1.
27 A. F. Cameron, D. W. Taylor and R. H. Nuttal, J. Chem. Soc. Dalton Trans., (1972) 1603.
28 S. Materazzi, K. Kurdziel, U. Tentolini, A. Bacaloni and S. Aquili, Thermochim. Acta, 395 (2003) 133.

DOI: 10.1007/s10973-007-8747-7